JOURNAL OF GUIDANCE, CONTROL, AND DYNAMICS
Vol. 31, No. 4, July–August 2008

Sensitivity of Cooperative Target Geolocalization to Orbit Coordination

Eric W. Frew*
University of Colorado, Boulder, Colorado 80302

DOI: 10.2514/1.32810

This article investigates the sensitivity of target geolocalization by a team of two unmanned aircraft to orbit coordination. Using an uncertain, deterministic target model, a nondimensional optimality criterion based on the Cramer–Rao lower bound of the geolocalization problem is defined. The optimal sensing configuration is specified by two parameters, allowing for a general sensitivity study using parameter sweeps of the range of the unmanned aircraft to the target and their transverse separation in a polar coordinate system fixed on the target. Orbit coordination to maintain the optimal configuration is often infeasible given limitations on unmanned aircraft dynamics, motion of the target vehicle, and background wind. Therefore, orbit coordination policies that trade angular separation for range must be used. The sensitivity analysis of the optimal configuration is extended to orbit coordination over a finite time horizon for static and constant-velocity targets. Three orbit coordination policies (one that maintains angular separation while allowing range to the target to vary, one that maintains range while allowing angular separation to vary, and one that allows both angular separation and range to vary) are compared against an ideal policy that maintains the optimal configuration for all time. The sensitivity analysis performed here shows that different orbit coordination policies should be applied in different sensor regimes. However, policies that maintain the optimal range while allowing the angular separation to vary are more robust over the entire set of possible sensor characteristics than approaches that maintain optimal angular separation at the expense of range.

I. Introduction

PERSISTENT intelligence, surveillance, and reconnaissance (PISR) has emerged as one of the primary applications of teams of low-cost autonomous unmanned aircraft [1–4]. One particular example PISR application is the use of an unmanned aircraft system (UAS) to perform cooperative standoff line-of-sight (CSLOS) tracking of friendly and adversarial targets (Fig. 1) [3–6]. Distributing a team of unmanned aircraft (UA) around a moving target at a standoff distance provides sensor coverage when the target vehicle is uncooperative or highly agile [4], and improves geolocalization errors from bearing and range sensors [5] while limiting the exposure of the UA to threats. A salient feature of target geolocalization using bearing- and range-based sensors (e.g., electrooptical/infrared cameras or lidar) is the dependence of the measurement uncertainty (in terms of error variance) on the position of the sensor relative to the target. The influence of input parameters (e.g., sensor mobility) on nonlinear estimation problems, such as target geolocalization, can be exploited to derive optimal geometric configurations of teams of sensing platforms [7–9]. In practice, however, maintenance of optimal configurations is not feasible given constraints on the kinematics of typical fixed-wing aircraft. Evaluating the sensitivity of target geolocalization to orbit coordination enables the design of CSLOS tracking controllers that are robust to variations in the sensor measurement uncertainty and the dynamics of the targets being tracked.

The concept of using system inputs to improve the quality of information sensed by the system has been applied to a number of cooperative control problems [10–14]. Optimal input design (OID) and active sensing refer to a large subclass of problems driven by model-based estimation that rely on the calculation of observability or information measures (e.g., Fisher information matrix or mutual information) that are functions of input states [10,11,13–15]. Although the observability and performance (in terms of error covariance propagation) for linear systems are functions of the system matrices and initial conditions only, some nonlinear and distributed estimation problems can be influenced by input variables. Example applications include multisensor management through covariance control [16], trajectory design to improve bearings-only tracking [10,17], path planning to enable a robotic manipulator to grasp a delicate object [18], target tracking by active sensor networks [11,15], optimal cooperative reconnaissance [8,13], and collaborative perception by unmanned ground and aerial vehicle teams [19].

Various different PISR architectures have used optimal input design policies for the cooperative control of multiple unmanned aircraft. A hierarchical multivehicle reconnaissance architecture was presented in [2] that assigned tasks and planned trajectories based on minimizing the weighted sum of the uncertainty of a set of prioritized targets. Optimal solutions were presented, as well as a suboptimal decomposition using a heuristic approach. Optimal cooperative reconnaissance by multiple vehicles in the presence of high-risk zones and terminal constraints was investigated using the receding horizon control framework [13]. Likewise, optimal sensor trajectories for bearings-only tracking [10] and optimal cooperative UAS sensing using azimuth, range, and range rate sensors [8] have been studied. Decentralized surveillance by a team of unmanned aircraft and unmanned ground vehicles was achieved by greedy descent through a local information field [19]. Similar concepts were used for the planning of general active sensor networks tracking static and moving targets [14,15]. Finally, optimal input design was used to develop receding horizon control approaches for the exploration of unknown environments with passive, noncooperative sensing and for cooperative radio source localization [20–22].

An alternative approach to incorporating the optimal input design concepts directly in the cooperative control framework is to decompose the problem into a hierarchical structure based on underlying assumptions related to OID concepts. For target geolocalization by cooperating UAS, the optimal configuration consists of angular spacing about the target at the minimum allowable standoff distance (Sec. III). Thus, different tracking algorithms have been designed to coordinate UAS orbits without explicitly determining geolocalization errors. Control algorithms for

Received 14 June 2007; revision received 22 October 2007; accepted for publication 23 October 2007.

*Assistant Professor, Aerospace Engineering Sciences; eric.frew@colorado.edu. AIAA Member.

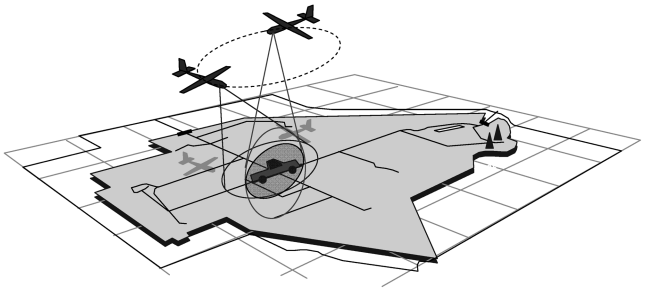

Fig. 1 Cooperative standoff line-of-sight tracking of a moving ground target by two cooperating unmanned aircraft.

the spacing of general oscillators (which can model UAS kinematics) about fixed points have been developed for an arbitrary number of agents [23]. The optimal phasing of two UAS orbiting at a fixed radius is used as one of the heuristics in the PISR architecture in [2]. Cooperative search, acquisition, and tracking of agile targets has also been performed by decoupling target assignment and orbit coordination based on desired angular separation between UAS [4]. Additionally, orbit coordination algorithms for tracking ground targets in the presence of wind attempt to regulate to the optimal tracking configuration [5].

One major drawback of tracking systems based on this type of hierarchical decomposition is the fact that maintaining the optimal configuration is often infeasible. Although the optimal configuration for geolocalization is straightforward to calculate using optimal input design concepts, optimal tracking of moving targets [4] in the presence of prevailing winds [5] is difficult, due to constraints on aircraft speeds and bank angles (which translate to aircraft turning rates). Thus, once it becomes infeasible to maintain the optimal configuration, CSLOS tracking controllers must trade optimal phasing with optimal standoff range. Several different CSLOS tracking approaches have been presented in the literature that use the optimal configuration as the basis for controllers that use suboptimal heuristics when optimal tracking becomes infeasible due to control input constraints. One approach, based on Lyapunov guidance vector fields and differential air speed, maintains the optimal standoff distance while allowing the relative phasing between two coordinating UAS to vary [4]. Alternatively, a second approach, based on good helmsman control, maintains the optimal phase separation between two orbiting UAS by allowing their standoff distances to change [3,5]. In both cases, the controllers were designed without considering the impact of the deviation from the optimal configuration on the underlying geolocalization problem.

This article investigates the sensitivity of cooperative target geolocalization by teams of UA to orbit coordination. The work presented in this article looks at the sensitivity of the target geolocalization problem to deviations from the optimal configuration to evaluate the performance of different CSLOS tracking approaches. A nondimensional optimality criterion is developed based on optimal input design concepts, specifically the Cramer–Rao lower bound and the Fisher information matrix. Using this nondimensional cost, its sensitivity to (nondimensionalized) deviations from the optimal configuration of aircraft at a given instant in time is determined as a function of the measurement error variances using parameter sweeps. Orbit coordination is evaluated by recursively calculating the optimality criterion over time. For static targets with no background wind, the optimality criterion is evaluated for different relative orbit configurations and compared with the ideal case where the vehicles maintain the optimal configuration at all times. Because regulation to the desired configuration is typically possible for aircraft, investigation of the static target case is independent of the specific orbit coordination policy. For moving targets and background wind, three orbit coordination policies (one that varies phase angle while fixing the standoff radius [4], one the varies the standoff range while fixing the phase separation [3,5], and one that combines the two concepts) are compared against an ideal controller which maintains the optimal configuration for all time.

The unique contribution of this article is the sensitivity analysis of target geolocation to several different orbit coordination strategies. Previous work developing orbit coordination policies for target geolocalization have only considered the ability of the aircraft to regulate to a desired relative configuration [3–5]. Unfortunately, that analysis failed to consider the ultimate goal of the orbit coordination policy: to improve or optimize the performance of the target geolocalization system. By considering the actual goal of the cooperating system, i.e., target geolocalization performance, the work presented here provides an assessment of different coordination policies for different sensor configurations. Three specific existing control policies are chosen as representative samples of the types of control strategies that can be employed. Several assumptions regarding the estimation process are made to generalize the sensitivity study. The resulting analysis provides guidelines for the selection of orbit coordination strategies based on the types of sensors that will be carried by the UA team. Although specific candidate control policies and geolocalization estimators should be analyzed before detailed conclusions can be drawn, the work presented here can be viewed as a design tool where the parameters describing the sensor system allow for tuning of the desired cooperation policies.

The remainder of this article is organized as follows. Section II presents the UA guidance models and orbit coordination policies compared here. Section III derives an optimality criterion based on the Cramer–Rao lower bound for the target geolocalization problem to derive the optimal configuration for two UA performing cooperative standoff line-of-sight tracking of a single ground target. Section IV investigates the sensitivity of target geolocalization to deviations from the optimal configuration at a given instant in time. Next, Sec. V evaluates three orbit coordination policies against the ideal configuration over extended time horizons. Finally, Sec. VI discusses the work presented here, and Sec. VII offers a summary and conclusion.

II. Unmanned Aircraft Guidance Model and Orbit Coordination Policies

This work assumes that UA are equipped with a low-level flight control system (FCS) that provides roll, pitch, and yaw stability of the aircraft, as well as velocity tracking and altitude-hold functions. For aircraft guidance, the FCS accepts speed, altitude, and turn-rate commands. Thus, the system model presented to the higher-level guidance layer (assuming constant altitude) is a kinematic model:

$$\dot{\mathbf{x}} = \begin{bmatrix} \dot{r} \\ r\dot{\theta} \\ \dot{\psi} \end{bmatrix} \equiv \begin{bmatrix} v_r \\ v_\theta \\ \dot{\psi} \end{bmatrix} = \begin{bmatrix} u_1 \cdot \cos(\psi - \theta) + v_w \cdot \cos(\psi_w - \theta) \\ u_1 \cdot \sin(\psi - \theta) + v_w \cdot \sin(\psi_w - \theta) \\ u_2 \end{bmatrix} \tag{1}$$

where $\mathbf{p} = [r, \theta]^T \in \Re \times [0, 2\pi)$ is the two-dimensional position of the aircraft in polar coordinates, $\psi \in [0, 2\pi)$ is the aircraft yaw angle, $\mathbf{x} = [\mathbf{p}^T, \psi]^T$ is the aircraft state, $\mathbf{v}_w = v_w \cdot [\cos\psi_w, \sin\psi_w]^T \in \Re^2$ is the background (horizontal) wind velocity in Cartesian coordinates, $\mathbf{u} = [u_1, u_2]^T \in \Re^2$ is the input vector with commanded airspeed u_1 restricted to $0 < v_{\min} \le u_1 \le v_{\max}$ and the commanded turn rate u_2 limited by $|u_2| \le \omega_{\max}$.

When expressed relative to a point $\mathbf{p}_t = [x_t, y_t]^T$ moving with speed $\mathbf{v}_t = v_t \cdot [\cos\psi_t, \sin\psi_t]^T \in \Re^2$ in Cartesian coordinates, the aircraft kinematic model in polar coordinates relative to the target becomes (see Fig. 2)

$$\dot{\mathbf{x}} = \begin{bmatrix} \dot{r} \\ r\dot{\theta} \\ \dot{\psi} \end{bmatrix} = \begin{bmatrix} u_1 \cdot \cos(\psi - \theta) + v_w \cdot \cos(\psi_w - \theta) - v_t \cdot \cos(\psi_t - \theta) \\ u_1 \cdot \sin(\psi - \theta) + v_w \cdot \sin(\psi_w - \theta) - v_t \cdot \sin(\psi_t - \theta) \\ u_2 \end{bmatrix} \tag{2}$$

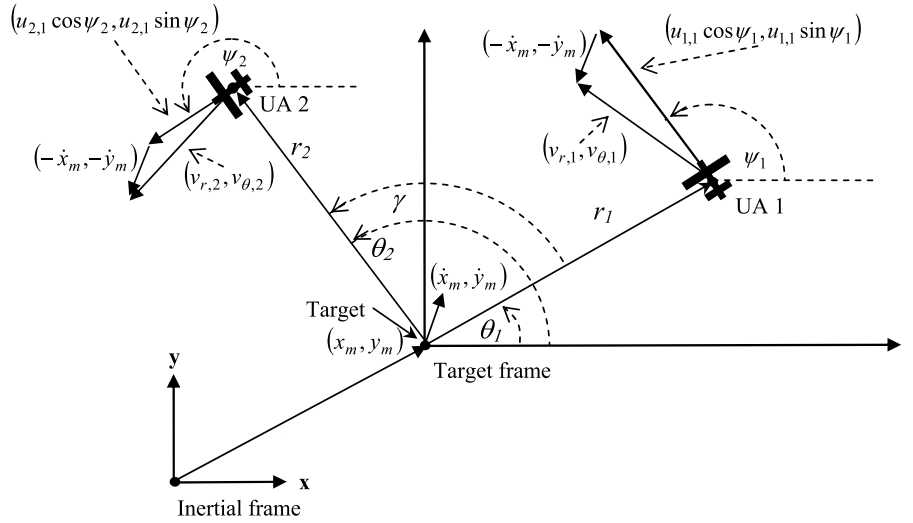

Fig. 2 Tracking geometry with ground target of interest at origin of the target frame.

Because the wind velocity and moving target velocity enter Eq. (2) in the same way, it is convenient to consider a single velocity term $\mathbf{v}_m = \mathbf{v}_t - \mathbf{v}_w = v_m \cdot [\cos\psi_m, \sin\psi_m]^T$. The remaining sections of this paper will refer to a *moving target* with the understanding that relative motion comes from the moving ground target and the background wind, i.e.,

$$\dot{\mathbf{x}} = \begin{bmatrix} \dot{r} \\ r\dot{\theta} \\ \dot{\psi} \end{bmatrix} = \begin{bmatrix} u_1 \cdot \cos(\psi - \theta) - v_m \cdot \cos(\psi_m - \theta) \\ u_1 \cdot \sin(\psi - \theta) - v_m \cdot \sin(\psi_m - \theta) \\ u_2 \end{bmatrix} \tag{3}$$

A discrete version of the aircraft kinematic model can be derived by assuming a zero-order hold on the inputs at times $t = t_0 + k \cdot T_s$, $k \in Z^+$, where Ts is the sample time, and integrating Eq. (3).

For this paper we consider orbit coordination of two unmanned aircraft which are referred to together as a single unmanned aircraft system with state $\mathbf{x}_k^{\text{UAS}} = [\mathbf{x}_{k,1}^T, \mathbf{x}_{k,2}^T]^T$ and input $\mathbf{u}_k^{\text{UAS}} = [\mathbf{u}_{k,1}^T, \mathbf{u}_{k,2}^T]^T$ at time k. The second subscripts in the variables denote the individual aircraft. The discrete update equation for the UAS is

$$\mathbf{x}_{k+1}^{\text{UAS}} = \mathbf{f}\left(\mathbf{x}_k^{\text{UAS}}, \mathbf{u}_k^{\text{UAS}}\right) = \begin{bmatrix} \mathbf{f}_1(\mathbf{x}_{k,1}, \mathbf{u}_{k,1}) \\ \mathbf{f}_2(\mathbf{x}_{k,2}, \mathbf{u}_{k,2}) \end{bmatrix} \tag{4}$$

where $\mathbf{f}_i(\mathbf{x}_{k,i}, \mathbf{u}_{k,i})$ is the discrete version of Eq. (3) applied to the ith aircraft.

Consider the case of perfect state information and define the control policy μ: $\Re^6 \to \Re^4$ as a function that maps the state of the UAS at time k to the control input $\mathbf{u}_k^{\text{UAS}} = \mu(\mathbf{x}_k^{\text{UAS}})$. Substituting the control policy back into Eq. (4) gives the closed loop state transition function $\mathbf{g}_\mu$: $\Re^6 \to \Re^6$ such that

$$\mathbf{x}_{k+1}^{\text{UAS}} = \mathbf{g}\left[\mathbf{x}_k^{\text{UAS}}, \mu\left(\mathbf{x}_k^{\text{UAS}}\right)\right] \equiv \mathbf{g}_\mu\left(\mathbf{x}_k^{\text{UAS}}\right) \tag{5}$$

The *trajectory* $\tau_{k:\ k+K}^{\mu}$ under control policy μ, over the time interval $[k, k+K]$, from initial condition $\mathbf{x}_k^{\text{UAS}}$ is defined as

$$\tau_{k:\ k+K}^{\mu} = \left[\mathbf{x}_k^{\text{UAS}}, \mathbf{x}_{k+1}^{\text{UAS}}, \ldots, \mathbf{x}_{k+K}^{\text{UAS}}\right] | \mathbf{x}_{k+1}^{\text{UAS}} = \mathbf{g}_\mu\left(\mathbf{x}_k^{\text{UAS}}\right) \tag{6}$$

Four different policies for coordinating the orbits of two UA will be discussed in this article. Each policy is parameterized by the desired standoff distance r_{des} from the target and the desired angular phase separation γ_{des} of the two UA around the target. The coordination policies are then based on the strategy of regulating the UA configuration to the desired one. Although regulation to the desired configuration is possible for a stationary target, and achievable by all policies, constraints on UA airspeed and turn rate often prevent convergence to the desired configuration when orbiting a moving target [4] or in the presence of wind [5]. Thus, the different coordination policies presented here trade standoff distance with phase separation. It should be noted that although this article considers coordination of two UA only, the control policies described next and the analysis of the optimal configuration in Sec. III could be expanded to include more vehicles. However, Ousingsawat and Campbell [13] conclude that the incremental improvement in geolocalization performance by adding a third vehicle is much less than that of adding a second, and that, whenever possible, the third (or more) vehicle is best used tracking additional targets.

The first control policy μ_{gvf} uses a modified guidance vector field (GVF) to achieve standoff tracking given control input constraints and target or wind velocity [4]. The GVF directs each UA onto a circular loiter pattern with the specified radius $r_{\text{des},i}$ by defining the desired UA velocity in polar coordinates as

$$\begin{aligned} \text{gvf}_{k,i}(\mathbf{x}_{k,i}, \mathbf{u}_{k,i}, r_{i,\text{des}}) &= \begin{bmatrix} v_r \\ v_\theta \end{bmatrix}_{k,i,\text{des}} \\ &= \frac{\alpha(r_{k,i}, \theta_{k,i}, u_{k,i,1}) \cdot u_{k,i,1}}{r_{k,i}^2 + r_{i,\text{des}}^2} \cdot \begin{bmatrix} -\left(r_{k,i}^2 - r_{i,\text{des}}^2\right) \\ 2 \cdot r_{k,i} \cdot r_{i,\text{des}} \end{bmatrix} \end{aligned} \tag{7}$$

where α is a scaling factor used to satisfy the airspeed constraints [4]. This scale factor is calculated by solving $\|\text{gvf}_{k,i} + \mathbf{v}_m\|^2 = u_{k,i,1}^2$, which has a single positive real root when $\|\mathbf{v}_m\| < u_{k,i,1}$, i.e., the UA is faster than the target. The UA turn rate $u_{k,i,2}$ is commanded using reference tracking control to follow this desired vector, i.e.,

$$u_{k,i,2} = \dot{\psi}_{k,i,\text{des}} - k_a(\psi_{k,i} - \psi_{k,i,\text{des}}) \tag{8}$$

where $\psi_{k,i,\text{des}}$ and $\dot{\psi}_{k,i,\text{des}}$ are the desired heading angle and turn rate that can be calculated from Eq. (7), and k_a is a control gain. Relative phasing between orbiting UA is achieved using speed commands given by

$$\begin{aligned} u_{k,1,1} &= k_p \frac{r_{k,1,\text{des}}^2}{r_{k,1}^2}(\gamma_k - \gamma_{\text{des}}) \cdot r_{1,\text{des}} + u_{1,\text{nom}} \\ u_{k,2,1} &= -k_p \frac{r_{k,2,\text{des}}^2}{r_{k,2}^2}(\gamma_k - \gamma_{\text{des}}) \cdot r_{2,\text{des}} + u_{1,\text{nom}} \end{aligned} \tag{9}$$

where $\gamma_k = \theta_{k,2} - \theta_{k,1}$ is the angular phase separation of the UA, γ_{des} is the desired phasing, k_p is a control gain, and $u_{1,\text{nom}}$ is the nominal UA speed. The overall behavior of this control policy is to give up relative phasing while maintaining the desired standoff distance from each UA to the target [4].

The second control policy μ_{rad} maintains the desired phase angle by allowing the UA to change their range from the target. In the first

step of the policy implemented here, the GVF approach of Eq. (7) is used to calculate the desired velocity for each UA. The transverse components of this velocity are compared and the range of the faster vehicle is increased such that the angular velocities between each UA and the target are equal. Letting

$$i_{\max} = \arg\max_{i\in\{1,2\}} v_{\theta,k,i,\text{des}} \qquad i_{\min} = \arg\min_{i\in\{1,2\}} v_{\theta,k,i,\text{des}} \tag{10}$$

be the indices of the UA with maximum and minimum transverse speed components, respectively, the radius of the UA with maximum speed (i.e., labeled with $i_{\max}$) is set to

$$r_{k,i_{\max}} = r_{\text{des}} \frac{v_{\theta,k,i_{\max},\text{des}}}{v_{\theta,k,i_{\min},\text{des}}} \tag{11}$$

In this case, the turn rate and speed constraints of the UA are ignored by "placing" the vehicles at the derived ranges. The velocity of the slower vehicle is calculated from the GVF approach and thus satisfies the control input constraints. In other words, for each sample time, the control policy of one UA satisfies the control constraints, while one policy may violate them. This constraint violation is allowed because it enables comparison against the ideal radial displacement. Setting the radius of the UA with maximum transverse speed according to Eq. (11) yields $\dot{\gamma}_k = \dot{\theta}_{k,2} - \dot{\theta}_{k,1} = 0$, and $\gamma_k = \gamma_{k-1}$ stays at the desired configuration if initialized there.

The third control policy $\mu_{\text{gvf}_{\text{rad}}}$ combines the first two policies in the same spirit as the controller described in [6]. The standoff distance for each UA is derived from the second control policy μ_{rad}. The resulting radii for each UA are then used as the commanded standoff distances for the Lyapunov guidance vector field algorithms in Eq. (7)

$$\begin{aligned}\begin{bmatrix} v_r \\ v_\theta \end{bmatrix}_{k,i_{\max},\text{des}} &= \text{gvf}_{k,i_{\max}}(\mathbf{x}_{k,i_{\max}}, \mathbf{u}_{k,i_{\max}}, r_{k,\text{rad}}) \\ \begin{bmatrix} v_r \\ v_\theta \end{bmatrix}_{k,i_{\min},\text{des}} &= \text{gvf}_{k,i_{amin}}(\mathbf{x}_{k,i_{\min}}, \mathbf{u}_{k,i_{\min}}, r_{\text{des},i_{\min}})\end{aligned} \tag{12}$$

where $r_{k,\text{rad}}$ is the radius determined by Eq. (11) for μ_{rad}. By commanding the standoff radii rather than placing the UA at them, this control policy respects the turn rate and speed constraints of the UA. Unlike the control policy in [6], the algorithm used here for $\mu_{\text{gvf}_{\text{rad}}}$ does not vary the desired phase separation with relative position.

The final control policy considered in this article is the ideal control policy μ_{ideal}. Under the ideal policy, the UA always maintain the desired configuration:

$$[r_{k,1}, r_{k,2}, \gamma_k] = [r_{\text{des}}, r_{\text{des}}, \gamma_{\text{des}}] \quad \forall\ k \tag{13}$$

Because it is not possible to achieve the ideal policy in practice, due to constraints on vehicle turn rate and airspeed [5], this policy is realized through direct specification of the closed loop state transition function and is only used for comparison. In this case, the ideal control policy is not necessarily unique because γ_{des} only describes the difference in phase of the two UA, however, it will be shown in Sec. III that geolocalization performance depends on this difference. This policy is referred to as the "ideal" policy as opposed to the "optimal" one because it ignores the control limitations imposed by the dynamic model in Eq. (1).

Figure 3 shows example trajectories using the first three control policies. In each case, the UA start with initial states [300 m, 0 m, 1.05 rad] and [0 m, 300 m, 3.14 rad], UA airspeed is $15 \le u_{i,1} \le 25$ m/s, the maximum turn rate is 0.2 rad/s, the desired standoff radius is 300 m, desired phase separation is $\pi/2$ rad, the target starts at the origin, and the target velocity is [10, 0] m/s. Table 1 lists the maximum and minimum phase angle separation between the two UA and the maximum range (in all cases, the minimum range is the desired range 300 m) of each UA for each scenario. As designed, control policy μ_{gvf} maintains the desired standoff distance while allowing phase separation to oscillate. By comparison, control policy μ_{rad} maintains the desired phase separation while allowing range to change. Finally, the tracking performance of control policy $\mu_{\text{gvf}_{\text{rad}}}$ is between the previous two policies. The standoff distance does not vary as much as when using μ_{rad}, and oscillation of phase separation is not as great as μ_{gvf}.

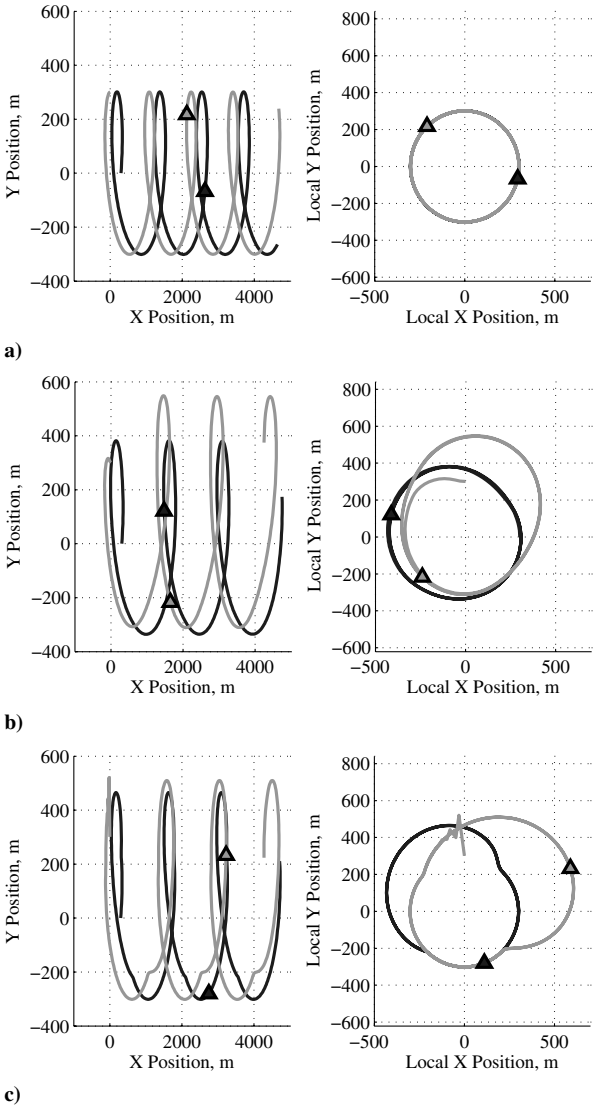

Fig. 3 Tracking a target starting at the origin, moving with velocity [10, 0] m/s using control policy a) μ_{gvf}, b) $\mu_{\text{gvf}_{\text{rad}}}$, and c) μ_{rad}. Markers denote snapshots of position of UA at points of maximum deviation.

Comparison of similar control policies under a wider variety of conditions is presented in [6], although the specific results presented in Fig. 3 and Table 1 are not included. In addition to the trends shown here between the three control policies, those results show that regulation errors (i.e., max / min deviations from the desired configuration) decrease as the desired phase separation γ_{des} decreases. Unfortunately, the results in [6] only characterize the tracking performance of different orbit coordination policies relative to the desired configuration. That approach is incomplete because the discussion does not include the actual goal of orbit coordination: target geolocalization. The effect of orbit coordination on

Table 1 Deviations from optimal configuration

Policy	Min γ, deg	Max γ, deg	Max r_1, m	Max r_2, m
μ_{gvf}	56.6	147.1	300.0	300.0
$\mu_{\text{gvf}_{\text{rad}}}$	58.1	100.5	440.5	556.8
μ_{rad}	90.0	90.0	488.8	634.8

geolocalization performance is discussed in the remainder of this article.

III. Optimal Cooperative Geolocalization

The impact of UA motion on geolocalization performance is characterized by the Cramer–Rao lower bound (CRLB). Although various nonlinear estimation schemes exist for target geolocalization [24–26], and they could be analyzed individually, the Cramer–Rao lower bound is used here because it describes the best possible estimator performance that can be obtained and therefore generalizes the results. The CRLB gives the following limit on the performance of any nonlinear estimator

$$\mathbf{P}_k \geq \mathbf{J}_k^{-1} \tag{14}$$

where $\mathbf{P}_k$ is the target state estimate error covariance matrix and $\mathbf{J}_k$ is the Fisher information matrix (FIM) at time k [27]. It is shown in [27] that the FIM for an unknown, deterministic variable with additive Gaussian white noise with covariance matrix $\mathbf{R}_k$ can be obtained by the recursive relationship

$$\mathbf{J}_k = \left(\mathbf{\Phi}_{k-1} \cdot \mathbf{J}_{k-1}^{-1} \cdot \mathbf{\Phi}_{k-1}^T\right)^{-1} + \mathbf{H}_k^T \cdot \mathbf{R}_k^{-1} \cdot \mathbf{H}_k \tag{15}$$

where the matrices $\mathbf{\Phi}_{k-1}$ and $\mathbf{H}_k$ are linearizations of the state transition function and measurement function, respectively, with respect to the state variables to be estimated (the inertial target position and velocity in this case). The recursion is initialized with $\mathbf{J}_0 = \mathbf{P}_0^{-1}$. When the measurement vector can be written as the concatenation of smaller vectors with independent noise, i.e., $\mathbf{z}_k = [\mathbf{z}_{k,1}, \ldots, \mathbf{z}_{k,N}]$ and $\mathbf{R}_k = \text{diag}[\mathbf{R}_{k,1}, \ldots, \mathbf{R}_{k,N}]$, then Eq. (15) becomes

$$\mathbf{J}_k = \left(\mathbf{\Phi}_{k-1} \cdot \mathbf{J}_{k-1}^{-1} \cdot \mathbf{\Phi}_{k-1}^T\right)^{-1} + \sum_{i=1}^{N} \mathbf{H}_{k,i}^T \cdot \mathbf{R}_{k,i}^{-1} \cdot \mathbf{H}_{k,i} \tag{16}$$

Equation (16) is useful when the vectors $\mathbf{z}_{k,i}$ represent measurements taken from different sensors (Fig. 4).

This work considers two-dimensional problems in which the UA know their own inertial locations, they are equipped with sensors that measure the bearing angle and range to a target, and the geolocalization system must estimate the inertial position of a static target or the inertial position and velocity of a moving target. The measurement taken by the ith UA is

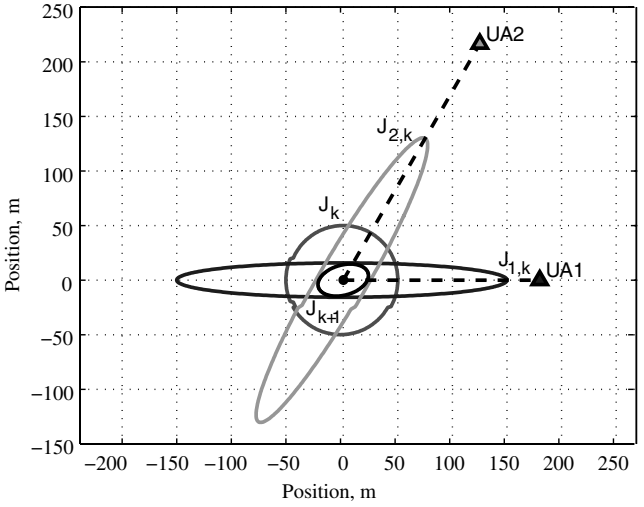

Fig. 4 Example results from FIM recursion with $\sigma_r = 150$ m and $\sigma_\theta = 4$ deg.

$$\mathbf{z}_{k,i} = h(\mathbf{x}_{k,i}, \mathbf{x}_{k,t}) + \mathbf{v}_{k,i} = \begin{bmatrix} r_{k,i} \\ \theta_{k,i} \end{bmatrix} + \mathbf{v}_{k,i} = \begin{bmatrix} \sqrt{(x_{k,t} - x_{k,i})^2 + (y_{k,t} - y_{k,i})^2} \\ \tan^{-1}\left(\frac{y_{k,t} - y_{k,i}}{x_{k,t} - x_{k,i}}\right) \end{bmatrix} + \mathbf{v}_{k,i} \tag{17}$$

where $[x_{k,t}, y_{k,t}]^T \in \Re^2$ is the inertial position of the target object in Cartesian coordinates, $[x_{k,i}, y_{k,i}]^T$ is the inertial position of the ith UA in Cartesian coordinates, and $\mathbf{v}_{k,i} \in \Re^2$ is white noise with uncorrelated variances σ_R^2 and σ_θ^2 in the range and bearing measurements, respectively (which is assumed to be the same for each UA at all times). Note that the second element of the measurement equation, referred to here as the bearing measurement, is actually the transverse position of the UA relative to the target in polar coordinates. "Bearing" also refers to the transverse position of the target relative to the y axis or the angular displacement of the target relative to the velocity vector of the vehicle. However, if the position and velocity of the UA is known, these other measurements can easily be converted into the measurement used here. The measurement equation [Eq. (17)] can describe many different types of sensors. Taking $\sigma_R^{-2} = 0, \sigma_\theta^2 < \infty$ models passive noncooperative (i.e., bearings only) sensing such as electrooptical/infrared cameras or passive sonar. On the other hand, taking $\sigma_R^2 < \infty, \sigma_\theta^{-2} = 0$ models pure trilateration, e.g., using some types of radar. Finally, conventional radar systems include both bearing and range measurements and would have finite values for both variances. It should be noted that for other sensor systems, such as sonar, σ_R^2 is a function of range to the object and has a "sweet spot" of minimum variance [7]. These types of sensors are not considered here. The sensor model can also be augmented with maximum range and field of view limitations, although it is assumed here that the target is always in view, e.g., using a gimbal.

The assumption that the components of the sensor noise vector $\mathbf{v}_{k,i}$ are uncorrelated Gaussian white noise are made here to simplify the analysis and emphasize the differences in geolocalization performance when using range-only or bearing-only sensing. This is common practice for information-theoretic analysis and design of mobile sensor platforms [7,8,13,14,19]. If more detailed analysis is needed for a specific system, the Fisher information matrix can be calculated for general systems with correlated, non-Gaussian sensor noise [27]. However, such calculations would be difficult to generalize for the sake of comparison. In the context of general nonlinear sensor systems, the work presented here can be used as a design tool to guide the selection of the orbit coordination policy. In that case, the variances of the sensor noise components can be interpreted as parameters to use to tune the design process.

For the sensor model of Eq. (17), the matrix $\mathbf{H}_{k,i}$ is

$$\mathbf{H}_{k,i} = \begin{bmatrix} \cos\theta_{k,i} & \sin\theta_{k,i} \\ \frac{1}{r_{k,i}}\sin\theta_{k,i} & -\frac{1}{r_{k,i}}\cos\theta_{k,i} \end{bmatrix} \tag{18}$$

Given two UA and a single target, the measurement component of the Fisher information matrix in Eq. (16) becomes

$$\sum_{i=1}^{2} \mathbf{H}_{k,i} \cdot R_{k,i}^{-1} \cdot H_{k,i}^T = \sum_{i=1}^{2} \begin{bmatrix} \frac{\cos^2\theta_{k,i}}{\sigma_R^2} + \frac{\sin^2\theta_{k,i}}{r_{k,i}^2\sigma_\theta^2} & \frac{\cos\theta_{k,i}\sin\theta_{k,i}}{\sigma_R^2} - \frac{\cos\theta_{k,i}\sin\theta_{k,i}}{r_{k,i}^2\sigma_\theta^2} \\ \frac{\cos\theta_{k,i}\sin\theta_{k,i}}{\sigma_R^2} - \frac{\cos\theta_{k,i}\sin\theta_{k,i}}{r_{k,i}^2\sigma_\theta^2} & \frac{\sin^2\theta_{k,i}}{\sigma_R^2} + \frac{\cos^2\theta_{k,i}}{r_{k,i}^2\sigma_\theta^2} \end{bmatrix} \tag{19}$$

Because the CRLB provides a lower bound on estimator performance, independent of the specific filter implementation, minimizing a measure of the CRLB for a system will often minimize the uncertainty in any specific estimation process. Equivalently, the FIM describes the amount of information a set of measurements contains about the state variable in terms of the sensitivity of the estimation process. Maximizing the FIM, i.e., providing better sensitivity, is more likely to improve the estimator performance and

reduce uncertainty. Control policies that yield large values of some measure of the FIM are expected to yield better estimation performance compared to policies that give lower values. Thus, the FIM can be used to compare the expected estimation performance that results from applying different control policies. Note, this use of the FIM is in contrast to optimal input design and active sensing techniques that determine system inputs directly to optimize a measure of the FIM [10,28].

A typical policy for cooperative target geolocalization using unmanned aircraft is to attempt to loiter around the target in some fixed relative configuration [3,4,6]. This configuration is specified in advance based on active sensing principles and then vehicle guidance and control attempts to maintain it. In particular, this configuration is typically determined by maximizing the information in the current measurements only without considering previous information or information that can be gained over some future finite time interval. That is, these guidance algorithms are designed to regulate to a configuration at time k, given (or assuming) no prior information at time $k-1$. If prior information is always ignored, then $\mathbf{J}_{k-1} = 0$ and Eq. (16) becomes

$$\mathbf{J}_k = \sum_{i=1}^{N} \mathbf{H}_{k,i} \cdot \mathbf{R}_{k,i}^{-1} \cdot \mathbf{H}_{k,i}^{T} \tag{20}$$

which, for the example considered in this article, is given by Eq. (19). One benefit of using Eq. (20) to calculate the desired relative configuration is that it is independent of the target motion model, which would be included in the state transition matrix.

Because of its popularity [7,13,14,28] and relatively low computational cost, this work uses the determinant $\eta_D(\mathbf{J}) = \det(\mathbf{J})$, referred to as the D-optimality criterion, to quantify the size of the FIM. [Though not shown here, it should be noted that the optimal configuration derived for the D-optimality criterion also optimizes the minimum eigenvalue (E-optimality criterion) and trace (A-optimality criterion) of the FIM.] Taking the determinant of Eq. (19) and applying several trigonometric identities gives

$$\eta_D(\mathbf{J}_k) = \eta_D(r_{k,1}, \theta_{k,1}, r_{k,2}, \theta_{k,2}) = \frac{1+\cos^2\gamma_k}{\sigma_R^2\sigma_\theta^2}\left(\frac{1}{r_{k,1}^2} + \frac{1}{r_{k,2}^2}\right) + \sin^2\gamma_k\left(\frac{1}{\sigma_R^4} + \frac{1}{\sigma_\theta^4 r_{k,1}^2 r_{k,2}^2}\right) \tag{21}$$

Equation (21) shows that the FIM is only a function of the angular separation between the two UA and not their transverse positions.

For $\sigma_R^2 \le \infty$ and $\sigma_\theta^2 < \infty$, the configuration that maximizes the optimality criterion is

$$[r_1^*, r_2^*, \gamma^*] = \arg \max_{\substack{\{r_{k,1}, r_{k,2}\} \in [r_{\min}, \infty) \\ \gamma_k \in [0,\pi]}} \eta_D(r_{k,1}, r_{k,2}, \gamma_k) = [r_{\min}, r_{\min}, \pi/2] \tag{22}$$

and

$$\eta_D^* = \max_{\substack{\{r_{k,1}, r_{k,2}\} \in [r_{\min}, \infty) \\ \gamma_k \in [0,\pi]}} \eta_D(r_{k,1}, r_{k,2}, \gamma_k) = \left(\frac{1}{\sigma_R^2} + \frac{1}{r_{\min}^2\sigma_\theta^2}\right)^2 \tag{23}$$

where $r_{\min}$ is the minimum allowable distance between the UA and the target. It is assumed that the same minimum distance applies to each UA and is set by safety and stealth considerations.

For $\sigma_\theta^{-2} = 0$ (i.e., pure ranging), the D-optimality criterion reduces to

$$\eta_D(\mathbf{J}_k) = \frac{\sin^2\gamma_k}{\sigma_R^4} \tag{24}$$

which is independent of the range from either UA to the target. The optimal configuration is therefore independent of range, however, the optimal phase angle separation is still $\gamma^* = \pi/2$.

IV. Geolocalization Sensitivity to Configuration

This section investigates the sensitivity of the FIM optimality criterion to changes in the relative phase angle between orbiting UA and to changes in the orbit radius of one of the UA. We assume one UA always stays at the desired standoff distance and that the second modifies its range (when appropriate) to achieve the desired spacing. Because the each UA contributes equally to the optimality criteria [i.e., Eq. (21) is symmetric with respect to r_1 and r_2], without loss of generality, we set $r_1 = r_{\min}$ and allow r_2 (set to $r = r_2$ for simplicity) to vary. Furthermore, we consider only the difference in phase $\gamma = \theta_2 - \theta_1$ between the UA without needing to know explicitly the transverse position θ_i of either vehicle. Finally, the subscript k is dropped from the variables for simplicity.

The sensitivity of the optimality criterion to the orbit parameters of the second UA can be approximated by linearizing Eq. (21) about the optimal configuration, yielding

$$\eta_D(r^*, r^* + \Delta r, \gamma^* + \Delta\gamma,) \approx \eta_D^* + \frac{\partial \eta_D}{\partial \gamma} \cdot \Delta\gamma + \frac{\partial \eta_D}{\partial r} \cdot \Delta r \tag{25}$$

where

$$\frac{\delta\eta_D}{\delta\gamma}(r^*, r^*, \gamma^*) = 2\sin\gamma\cos\gamma\left(\frac{1}{\sigma_R^4} + \frac{1}{\sigma_\theta^4 r_{\min}^2 r^2} + \frac{1}{\sigma_R^2\sigma_\theta^2 r_{\min}^2} + \frac{1}{\sigma_R^2\sigma_\theta^2 r^2}\right)\Bigg|_{r_1=r_2=r^*, \gamma=\gamma^*} = 0 \tag{26}$$

and

$$\frac{\delta\eta_D}{\delta r}(r^*, r^*, \gamma^*) = -2\left(\frac{1+\cos^2\gamma}{\sigma_R^2\sigma_\theta^2 r^3} + \frac{\sin^2\gamma}{\sigma_\theta^4 r_{\min}^2 r^3}\right)\Bigg|_{r_1=r_2=r^*, \gamma=\gamma^*} = \frac{-2}{\sigma_\theta^2 r_{\min}^3}\left(\frac{1}{\sigma_R^2} + \frac{1}{\sigma_\theta^2 r_{\min}^2}\right) \tag{27}$$

From these expressions, it is clear that for small deviations in phase angle the optimality criterion is unchanged, whereas for small changes in range (away from the target) the optimality criterion is reduced, except when $\sigma_\theta^{-2} = 0$, in which case the sensitivity to range is also zero. Unfortunately, this analysis is incomplete because wind and target motion can cause large deviations from the optimal configuration, and Eq. (25) will not apply [4,5].

To generalize analysis, we define the nondimensionalized optimality criteria $\hat{\eta}_D$ by dividing both sides of Eq. (21) by η_D^*, letting $r_1 = r_{\min}$, and defining nondimensional terms $\hat{\gamma} = \gamma - \pi/2$, $\hat{r} = (r - r_{\min})/r_{\min}$, and $\hat{\sigma}^2 = r_{\min}^2\sigma_\theta^2/\sigma_R^2$, yielding

$$\hat{\eta}_D(\hat{r}, \hat{\gamma}) \equiv \frac{\eta_D(r^*, r^* + \hat{r}, \gamma^* + \hat{\gamma})}{\eta_D^*} = \frac{1}{(\hat{\sigma}^2+1)^2}\left[\hat{\sigma}^2(1+\sin^2\hat{\gamma})\left(1 + \frac{1}{(1+\hat{r})^2}\right) + \cos^2\hat{\gamma}\left(\hat{\sigma}^4 + \frac{1}{(1+\hat{r})^2}\right)\right] \tag{28}$$

The optimal nondimensional cost now has a value of one for nondimensional parameter values of zero. Note that multiplying $\hat{\gamma}$ or $\hat{r}$ by the optimal radius $r_{\min}$ gives the distance (around the circle or radially outward, respectively) of the second UA from the optimal configuration.

Figure 5 shows plots of the surface defined by Eq. (28) for different values of the nondimensional measurement standard deviation $\hat{\sigma}$. In Figure 5a, $\hat{\sigma} = 0.01$, effectively depicting bearings-only tracking because the range measurement has large uncertainty compared with the bearing measurement. In this case, $\hat{\eta}_D$ is sensitive to both $\hat{\gamma}$ or $\hat{r}$, and the performance degrades as $\hat{r}$ increases for all values of $\hat{\gamma}$, but increasing $\hat{\gamma}$ degrades performance to a point ($\hat{\gamma} = \pi/2$) after which

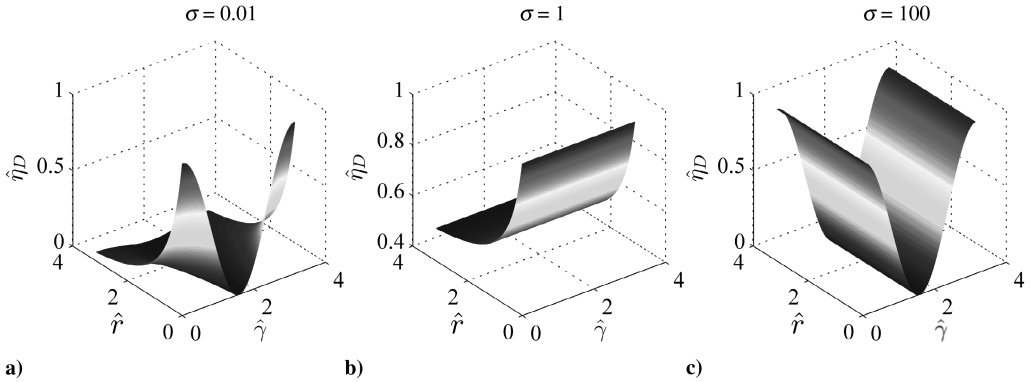

Fig. 5 Nondimensional cost η_D vs nondimensional radius and phase separation for different values of nondimensional sensor standard deviation.

it rises back toward the optimal value. In Figure 5b, $\hat{\sigma} = 1.0$, corresponding to circular uncertainty ellipsoids for each measurement. In this case, the relative phasing of the UAS has no effect on the optimality criterion but increases in range degrade performance. Finally, Figure 5c depicts the case where $\hat{\sigma} = 100.0$, corresponding closely to pure ranging. In this case, the uncertainty is independent of the range of the UAS to the target and therefore the optimality criterion is only a function of the relative phase angle.

Two additional nondimensional functions are defined by fixing $\hat{\gamma}$ (or $\hat{r}$) at its optimal value and allowing $\hat{r}$ ($\hat{\gamma}$) to vary:

$$\hat{J}_r(\hat{r}) \equiv \hat{\eta}_D(\hat{r}, \hat{\gamma} = 0) = \frac{1}{(\hat{\sigma}^2 + 1)^2}\left[\hat{\sigma}^2\left(1 + \frac{1}{(1+\hat{r})^2}\right) + \left(\hat{\sigma}^4 + \frac{1}{(1+\hat{r})^2}\right)\right] \tag{29}$$

and

$$\hat{J}_\gamma \equiv \hat{\eta}_D(\hat{r} = 0, \hat{\gamma}) = \frac{1}{(\hat{\sigma}^2 + 1)^2}[2\hat{\sigma}^2(1 + \sin^2\hat{\gamma}) + \cos^2\hat{\gamma}(\hat{\sigma}^4 + 1)] \tag{30}$$

Each function defined by Eqs. (29) and (30) has a minimum dependent on $\hat{\sigma}$ given as

$$J_r^*(\hat{\sigma}) = \min_{\hat{r}\in[0,\infty)} \hat{J}_r(\hat{r}) = \lim_{\hat{r}\to\infty} \hat{J}_r(\hat{r}) = \frac{\hat{\sigma}^2}{\hat{\sigma}^2 + 1} \tag{31}$$

and

$$J_\gamma^*(\hat{\sigma}) = \min_{\hat{\gamma}\in[0,\pi]} \hat{J}_\gamma(\hat{\gamma}) = \hat{J}_\gamma(\pi/2) = \frac{4\hat{\sigma}^2}{(\hat{\sigma}^2 + 1)^2} \tag{32}$$

Figure 6 shows plots of Eqs. (29) and (30) for different values of $\hat{\sigma}$. For $\hat{\sigma} \ll 1$ (which essentially describes bearings-only localization), the plot of $\hat{J}_r$ drops off steeper than the plot of $\hat{J}_\gamma$ (Figure 6a). As expected from Eqs. (26) and (27), the curve for the nondimensional radius (solid line) rapidly decreases monotonically from the optimal value (Fig. 6). By comparison, the curve for the phase angle (dashed line) has an initial slope of zero and starts to decrease more slowly. This curve reaches a minimum at a value of zero (no information), corresponding to an angle of $\pi/2$ rad (which means phase separation of π rad between UA and no triangulation) before rising back to the optimal value at π rad (total separation of $3\pi/2$ rad $= -\pi/2$ rad). Thus, for a given nondimensional distance, error in range degrades performance more than error in relative phase, up until a distance of approximately $\{\hat{\gamma}, \hat{r}\} = 1.1$. For $1.1 < \{\hat{\gamma}, \hat{r}\} < 1.8$, $\hat{J}_\gamma < \hat{J}_r$, and phase separation is worse than radial error. Figure 6b shows the case where $\hat{\sigma} = 1$. In this case, changes in $\hat{\gamma}$ have no effect on the geolocalization accuracy because the measurement contribution to the FIM is circular, whereas radial error decreases performance monotonically. Finally, for $\hat{\sigma} \gg 1$ (range-only localization) the radial error has no effect on performance, whereas changes in phase angle degrade performance (Figure 6c).

Figure 7 shows plots of the minima of Eqs. (29) and (30) vs $\hat{\sigma}$ [given by Eqs. (31) and (32)]. It can be seen that the maxima of Eqs. (29) and (30) are 1.0 for every $\hat{\sigma}$, thus Fig. 7 can indicate the dependence of the optimality criteria on $\hat{\gamma}$ or $\hat{r}$ at different values of $\hat{\sigma}$. For $\hat{\sigma} \gg 1.0$, the minimum value of $\hat{J}_r$ approaches 1.0, and so $\hat{J}_r \approx 1\ \forall\ \hat{r}$, i.e., the value of $\hat{J}_r$ in this region does not change with $\hat{r}$ and therefore $\hat{\eta}_D$ is only dependent on $\hat{\gamma}$. Likewise, $\hat{J}_\gamma = 1.0\ \forall\ \hat{\gamma}$ only for $\hat{\sigma} = 1.0$ (and therefore $\hat{\eta}_D$ is only dependent on $\hat{r}$). For $\hat{\sigma} \ll 1.0$, $\hat{\psi}_D$ is dependent on $\hat{r}$ and $\hat{\gamma}$, and so additional plots such as Figs. 5 and 6 are needed to understand the sensitivity of the geolocation estimation error. The importance of this sensitivity and these dependent regions in relation to cooperative target tracking is discussed further in Sec. V.

The overall implication of Figs. 5–7 is that information gain at a given time (and hence geolocalization performance) is more robust to phase angle separation than range over a wide set of sensor conditions (parameterized by $\hat{\sigma}$), and therefore maintaining optimal

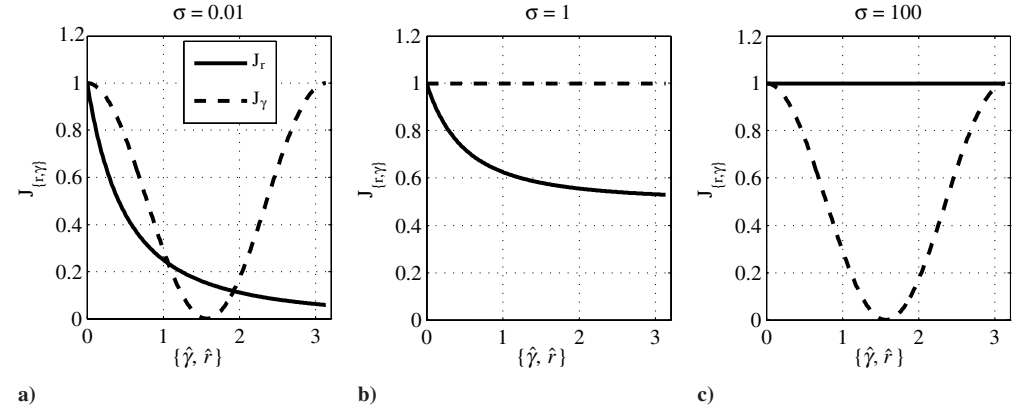

Fig. 6 Projections of (nondimensional) cost vs radius and phase separation for different values of $\hat{\sigma}$.

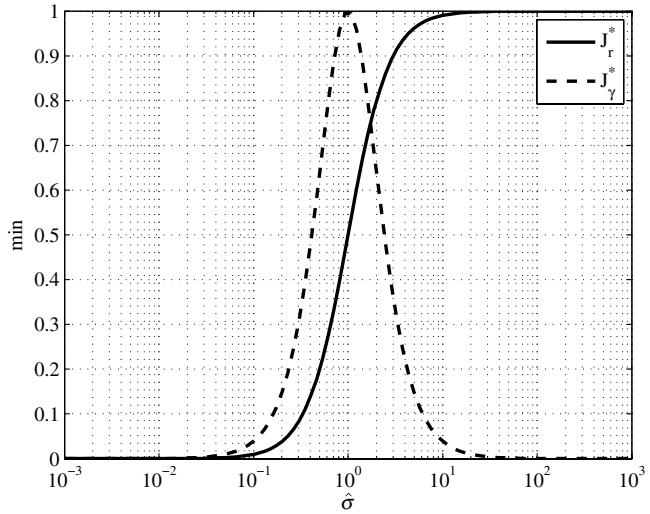

Fig. 7 Minimum values of $\hat{J}_\gamma$ and $\hat{J}_r$ vs the nondimensional standard deviation.

range to the target is preferred in general. This conclusion is most evident in Fig. 7, which shows that the geolocalization process is more robust to $\hat{\gamma}$ than $\hat{r}$ for $\hat{\sigma} \leq 2$, which on a logarithmic scale is more than half the domain. Further analysis in Sec. V on robustness to orbit coordination policies will show that even when maintaining range is preferable, the difference in performance compared with maintaining phase is much less than when maintaining phase is preferable.

V. Geolocalization Sensitivity to Orbit Coordination

Because unmanned aircraft cannot stop in place and instead orbit around a target, analysis of geolocalization performance bounds must consider the total amount of information collected over time. Cooperative standoff line-of-sight orbiting can be performed in the optimal configuration when the target of interest is slow moving compared with the air speed of the vehicle or when the desired standoff distance is large compared with the minimum radius of curvature (maximum turn rate) achievable by the vehicle. However, given typical constraints on the aircraft model, it becomes impossible to maintain the optimal configuration throughout an orbit [4,5]. Thus, different control policies (e.g., those presented in Sec. II) have been developed that trade standoff distance with relative phasing to stay within the feasible flight envelope [4,5]. The following sections investigate the sensitivity of cooperative geolocalization for static and moving targets.

A. Stationary Target

Consider a stationary target first sensed at time $k = 1$ with no prior information. Equation (16) is used to recursively calculate the Fisher information matrix $\mathbf{J}_k$ at time k with state transition matrix $\mathbf{\Phi}_k = \mathbf{I}_2 \ \forall\, k$ and initial condition $\mathbf{J}_0 = \mathbf{0}_2$, where $\mathbf{I}_2$ and $\mathbf{0}_2$ are the two-dimensional identity and zero matrices, respectively. A new nondimensionalized optimization criterion is defined as

$$\hat{\eta}_k = \frac{\eta_D(\mathbf{J}_k)}{\eta_k^{\text{ideal}}} = \frac{\eta_D(\mathbf{J}_k)}{k^2 \cdot \eta_D^*} \tag{33}$$

where η_k^{ideal} is the D-optimality criterion of the FIM that would result if the two UA maintained the optimal configuration for all time up to time k. It is trivial to show that $\eta_k^{\text{ideal}} = k^2 \cdot \eta_D^*$, where η_D^* is given by Eq. (23).

Although the optimal configuration can be achieved while orbiting around a stationary target [4,5], it is not clear that this is needed to obtain good tracking performance. Intuitively, the UA team will collect the same amount of information over a single orbit, given any fixed relative configuration at the minimum standoff distance. Thus, achieving optimal spacing may not be necessary if tracking persists over a long enough time horizon.

Geolocalization performance over time is compared for different orbit configurations. As in Sec. II, the lead UA is assumed to be on the desired loiter circle, whereas the position of the second UA is fixed at different offset values (again denoted $\hat{\gamma}$ and $\hat{r}$). Because each orbit coordination policy described in Sec. II is capable of meeting the desired configuration for the static case, μ_{gvf} is used to generate the results presented in this section. Simulations were run with standoff distance $r_{\min} = 300$ m, speed $v = 20$ m/s, and sample time $T_s = 1.0$ s, and the results are reported vs nondimensional time $\hat{t} = kT_s v / r_{\min}$. Figure 8 shows how Eq. (33) evolves over (nondimensional) time for different relative configurations for different values of the nondimensional measurement standard deviation. Figure 8a represents the time history of Eq. (33) for different values of $\hat{r}$, whereas Fig. 8b represents plots of Eq. (33) for different values of $\hat{\gamma}$. As expected, $\forall\, \hat{\gamma}$, $\forall\, \hat{\sigma}$, $\hat{r} = 0$ $\hat{\eta}_k \to 1$ as $k \to \infty$, implying that phase separation does not matter and optimal information gain is achieved if tracking occurs over a long enough time horizon. By comparison, when $\hat{\gamma} = 0$ $\hat{\eta}_k \to \eta_0(\hat{r}, \hat{\sigma}) \leq 1$ as $k \to \infty$. In other words, the information gain obtained when the standoff distance is greater than the minimum allowable distance never approaches the optimal value, except for pure trilateration (i.e., $\hat{\sigma} = \infty$). Although optimal information is gained in the limit for different specified angular spacings, the rise time of $\hat{\eta}_k$ is a function of phase separation.

Although the results of Fig. 8 show that maintaining the optimal range yields significantly more information over time for all measurement standard deviations, it is important to consider the absolute magnitude of the resulting uncertainty in these cases. To develop an intuitive measure of expected uncertainty, consider the square root of the maximum singular value of the CRLB, i.e., $\rho_{\max} = \sqrt{\sigma_{\max}(\mathbf{J}_k^{-1})}$. This value, which is in units of position, gives a measure of the maximum expected error in the distance between the estimate and the target. Figure 9 shows a plot of $\rho_{\max}$ for different values of $\hat{\gamma}$ and $\hat{r}$ for the specific values $\sigma_r = 52.35$ m and $\sigma_\theta = 1$ deg ($\hat{\sigma} = 0.1$). Figure 9a shows the plots of $\rho_{\max}$ vs time, whereas Fig. 9b shows the settling time (time to reach 2 m) vs $\{\hat{r}, \hat{\gamma}\}$. Although Fig. 8b shows that for $\hat{r} > 0$, $\hat{\gamma} = 0$, only a fraction of the optimal information is gained, Fig. 9a reveals that this corresponds to a difference of fractions of a meter in position error bounds. Furthermore, Fig. 9b shows that for all relative configurations, the square root of the maximum singular value of the CRLB is reduced to less than 2 m in 5–25 s. Thus, although fixing the standoff distance and allowing the phase separation to be nonoptimal is preferable to fixing the phase and changing the standoff distance, the optimal configuration only yields slightly faster settling times and final position uncertainty bounds compared with other configurations. Because the specific scenario ($\hat{\sigma} \ll 1$) investigated in Fig. 9 has the worst relative performance when comparing fixed phase or range, it is expected that similar results hold for other specific values of the sensor variances (although the specific final position bounds will change).

B. Moving Target

For the moving target scenario, we assume constant-velocity motion (which is independent of the UA motion) and have

$$\mathbf{\Phi}_k = \begin{bmatrix} 1 & 0 & T_s & 0 \\ 0 & 1 & 0 & T_s \\ 0 & 0 & 1 & 0 \\ 0 & 0 & 0 & 1 \end{bmatrix} \quad \forall\, k \tag{34}$$

where the target state $\mathbf{x}_t = [x_t, y_t, \dot{x}_t, \dot{y}_t]^t$ is being estimated and

$$\mathbf{H}_{k,i} = \begin{bmatrix} \cos\theta_{k,i} & \sin\theta_{k,i} & 0 & 0 \\ \frac{1}{r_{k,i}}\sin\theta_{k,i} & -\frac{1}{r_{k,i}}\cos\theta_{k,i} & 0 & 0 \end{bmatrix} \tag{35}$$

To consider the role of control policy μ on the information, again consider a target first seen at time $k = 1$ with initial uncertainty $\mathbf{P}_0$.

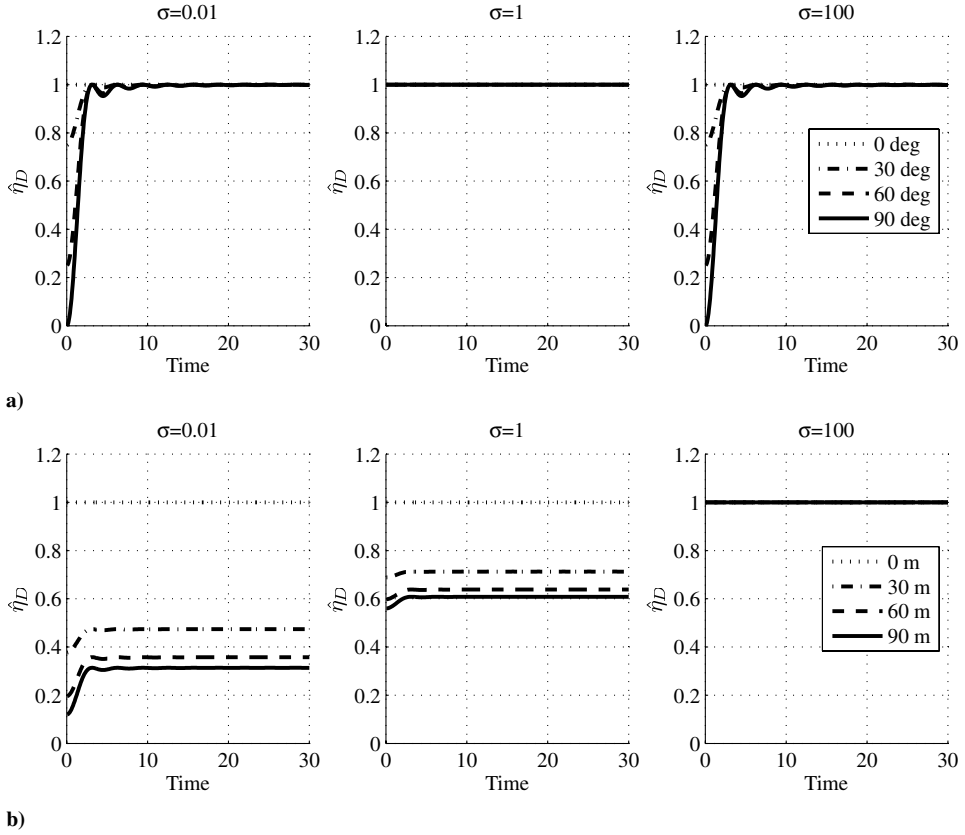

Fig. 8 Nondimensional cost $\hat{\eta}_D$ vs time $\hat{t}$ for different values of $\hat{\sigma}$ for different values of a) $\hat{\gamma}$ and b) $\hat{r}$.

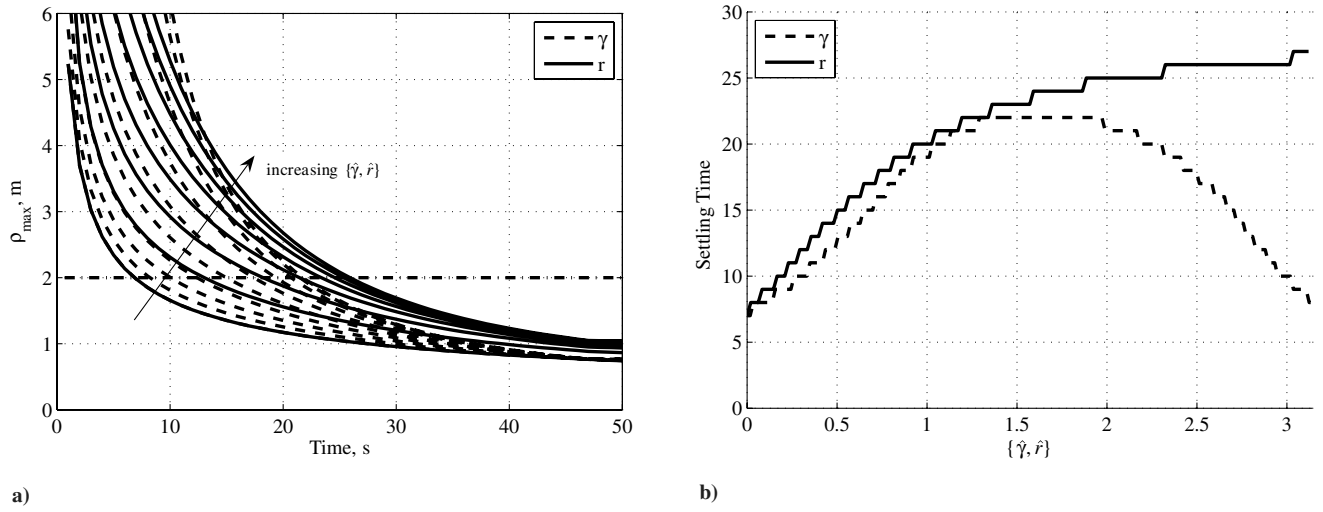

Fig. 9 Absolute magnitude of estimate uncertainty: a) maximum singular value ρ_{max}, and b) settling time for $\sigma_r = 52.35$ m and $\sigma_\gamma = 1$ deg ($\hat{\sigma} = 0.1$).

Because the measurement component

$$\sum_{i=1}^{2} \mathbf{H}_{k,i}^T \mathbf{R}_{k,i}^{-1} \mathbf{H}_{k,i}$$

of the FIM is singular for the moving target case, there must be a nonsingular initial information matrix $\mathbf{J}_0$ for the recursion of Eq. (16) to hold, thus

$$\mathbf{P}_0 = \begin{bmatrix} p_{\max}^2 \cdot \mathbf{I}_2 & \mathbf{0}_2 \\ \mathbf{0}_2 & v_{\max}^2 \cdot \mathbf{I}_2 \end{bmatrix} \tag{36}$$

where $p_{\max} = 1000$ m is the maximum initial position uncertainty and $v_{\max} = 100$ m/s is the maximum initial velocity uncertainty. Finally, define the new nondimensional optimality criterion

$$\hat{\eta}_k^{\,\mu} = \frac{\eta_D^{\mu}(\mathbf{J}_k)}{\eta_k^{\text{ideal}}} = \frac{\eta_D^{\mu}(\mathbf{J}_k)}{k^2 \cdot \eta_D^*} \tag{37}$$

to denote the optimality criterion as a function of time k for a given control policy μ. The term $\eta_D^{\mu}(\mathbf{J}_k)$ in Eq. (37) gives the D-optimality criterion of the FIM calculated when applying control policy μ, and the denominator again gives the FIM resulting from the ideal policy.

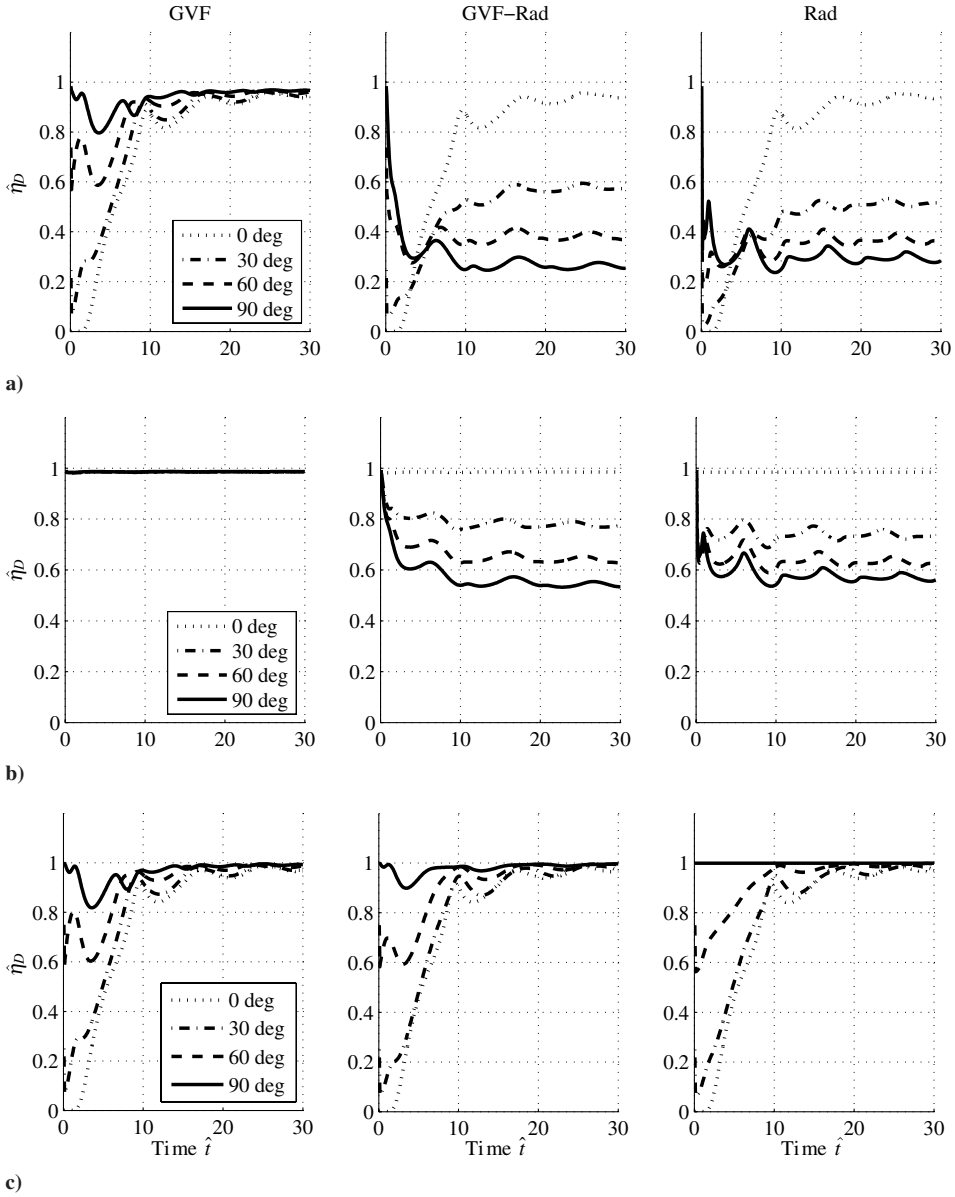

Fig. 10 Information cost vs time for different control policies: a) $\hat{\sigma} = 10^{-2}$, b) $\hat{\sigma} = 10^{0}$, and c) $\hat{\sigma} = 10^{2}$.

The three control policies μ_{gvf}, $\mu_{\text{gvf}_{\text{rad}}}$, and μ_{rad} are compared for different sensor configurations ($\hat{\sigma}$) and desired phase separation angles (γ_{des}). Figure 10 shows the time histories of the nondimensional optimality criterion for each control policy at different sensor configurations ($\hat{\sigma} = \{10^{-2}, 10^{0}, 10^{2}\}$) and separation angles ($\gamma_{\text{des}} = \{0, 30, 60, 90 \text{ deg}\}$). For bearings-only tracking ($\hat{\sigma} \ll 1$, shown in Fig. 10a), the Lyapunov vector field approach captures most of the available information after approximately three orbits (corresponding to nondimensional time $\hat{t} = 3 \cdot 2\pi \approx 19$), i.e., $\hat{\eta}_k^{\text{gvf}} \approx 1.0$ $k > 6\pi$, regardless of the desired angular separation γ_{des}. This result is consistent with expectations because, over an orbit, each UA takes measurements from all bearing angles to the target, and so relative phase separation is not critical. The performances of the other two control policies, which allow the range to the target to decrease to maintain the desired separation, vary greatly depending on the desired separation angle. Surprisingly, more information is gained from $\mu_{\text{gvf}_{\text{rad}}}$ and μ_{rad} when the desired separation distance is small (and thus far from the optimal spacing of 90 deg). This is due to the fact that the larger the desired separation distance, the more the range to the target of the second UA must be increased. For the case when the desired separation distance is zero (i.e., the two UA are at the same position), the optimal range can always be maintained and most of the information is captured after several orbits (see the middle and right plots of Fig. 10a).

The performance of the three control policies is similar to the bearings-only case when the measurement covariance is circular, i.e., when $\hat{\sigma} = 1.0$. In this case, the measurement component of the Fisher information matrix is independent of the relative phase separation so that $\hat{\eta}_k^{\text{gvf}} = 1.0 \ \forall \ k$. Following the same reasoning as the bearings-only case, the information gained from $\mu_{\text{gvf}_{\text{rad}}}$ and μ_{rad} is better for smaller values of γ_{des}. In this case,

$$\hat{\eta}_k^{\text{gvf}_{\text{rad}}} = \hat{\eta}_k^{\text{rad}} = 1.0 \quad \forall \ k$$

when $\gamma_{\text{des}} = 0.0$ deg.

The final case (Fig. 10c) shows the performance of the three control policies for range-only tracking ($\hat{\sigma} \gg 1$). In this case, there is no error in the bearing component of the measurement, and so the measurement component of the FIM is independent of the range of the UA to the target and therefore depends only on the relative phase separation between the two UA. The performance of μ_{gvf} (left plot of Fig. 10c) is nearly identical to that of the bearings-only case. Over the span of several orbits, the effects of deviations of the relative phase angle from the optimal configuration (due to oscillation from the

control policy and nonoptimal desired spacing) are reduced, and $\hat{\eta}_k^{\text{gvf}} \approx 1.0$ $k > 6\pi$. In contrast to the scenarios where $\hat{\sigma} \leq 1$, the policies $\mu_{\text{gvf}_{\text{rad}}}$ and μ_{rad} are also able to capture most of the information about the target after several orbits, regardless of the desired phase separation. Because the measurement contribution of the FIM is independent of range, only phase separation matters and, over the course of several orbits, measurements are taken from all bearing angles to the target. Furthermore, these policies work best when the desired angle is set to the optimal one, i.e., when $\gamma_{\text{des}} = 90.0$ deg, because the large increase in range needed to maintain the optimal separation angle does not change the information content in the measurements.

An alternate assessment of the different control policies is provided by comparing the final nondimensional information costs of each method as a function of sensor noise $\hat{\sigma}$. Figure 11 shows plots of $\hat{\eta}_{450}^{\mu}$ for each control policy under desired phase separations $\gamma_{\text{des}} = \{0.0, 90.0 \text{ deg}\}$. Figure 11 shows the information cost vs sensor standard deviation $\hat{\sigma}$. For $\hat{\sigma} < 10$, the best policy is μ_{gvf} with $\gamma_{\text{des}} = 90.0$ deg, and the policy achieves good performance with $0.95 < \hat{\eta}_{450}^{\text{gvf}} < 1$. When $\gamma_{\text{des}} = 0.0$ deg, all three policies achieve the same level of performance with $\hat{\eta}_{450}^{\mu} \approx 0.95$. This result is counterintuitive because the phase separation is far from the optimal value of $\gamma_{\text{des}} = 90.0$ deg. Likewise, when $\gamma_{\text{des}} = 90.0$ deg, $\mu_{\text{gvf}_{\text{rad}}}$ and μ_{rad} perform poorly, achieving $\hat{\eta}_{450}^{\mu} < 0.3$ over most of the sensor standard deviation range. In contrast, when $\hat{\sigma} > 10$, $\mu_{\text{gvf}_{\text{rad}}}$ and μ_{rad} perform the best, capturing most of the available information ($\hat{\eta}_{450}^{\mu} \approx 1.0$). Figure 11b shows a logarithmic plot of information cost error, relative to the ideal policy, vs $\hat{\sigma}$. It is clear from this plot that μ_{rad} performs best when $\hat{\sigma} > 10$ and that it continues to improve as $\hat{\sigma}$ increases, whereas the other policies all plateau. However, Fig. 11a shows that even when $\mu_{\text{gvf}_{\text{rad}}}$ and μ_{rad} perform better than μ_{gvf}, the Lyapunov guidance vector field control policy, which maintains optimal range at the expense of optimal phasing, still performs well with $\hat{\eta}_{450}^{\text{gvf}} > 0.99$.

VI. Discussion

The analysis provided in this paper shows that performance bounds for target geolocalization by two cooperating UA, as determined by the Fisher information matrix, is a strong function of the relative configuration between the aircraft and the target. Although the optimal configuration can easily be determined, it is not always possible to maintain this configuration, in the case of moving targets with background wind, nor is it necessary to achieve good results, e.g., when orbiting a stationary or constant-velocity target over a sufficient interval of time. The results of Secs. IV and V.A that show the robustness of geolocalization performance to errors from the optimal configuration are general, i.e., they are independent of specific orbit coordination schemes. In contrast, the analysis provided for the moving target case in Sec. V.B was for several specific orbit coordination policies; however, given the explanation of these results, one expects the overall trends to generalize to different classes of controllers, specifically, to orbit coordination policies that increase range to the target to maintain optimal angular separation, and to policies that vary separation angle to maintain the optimal range to the target.

The main parameter that determined the sensitivity of target geolocalization to orbit coordination was the nondimensionalized sensor error standard deviation $\hat{\sigma}$ which quantifies the ratio of range and bearing sensor noise variances. Results showed that, for different sensor regimes (particularly for bearings-only $\hat{\sigma} \ll 1$, circular $\hat{\sigma} = 1$, and range-only $\hat{\sigma} \gg 1$ sensing), different orbit coordination policies with different parameter values for the desired angular separation are suitable. However, overall behavior across all values of $\hat{\sigma}$ was better for control policies that maintain range while allowing the phase separation to vary away from the optimal value. Even in situations when the alternative policies performed better, the overall error compared with the ideal control policy was close to 1%. Thus, if a single orbit coordination algorithm must be designed for a UA that could carry sensors of varied capability, maintaining optimal range at the expense of phasing is preferred.

The sensitivity results provided here are best used as a guide for developing cooperative orbit coordination policies for two unmanned aircraft. Use of the Fisher information matrix for sensor system design is common [7,8,13,14,19] because it describes the "information content" that can be provided to estimation subsystems. The common assumption is that with more information, the estimation subsystem will determine a better, more accurate estimate of the system. For cooperative target tracking, optimal configuration design is insufficient because the UA are not able to maintain a single configuration under typical operating conditions and constraints. Therefore, sensitivity of the optimal configuration must also be considered.

As a design tool, the results provided here give insight into two complementary design decisions. First, for a given sensor configuration, the sensitivity analysis can be used to determine a control strategy. For bearings-only sensing, it is preferable to maintain range at the expense of angular separation, whereas for range-only sensing, the opposite is true. Furthermore, if the control policy is also fixed, the analysis gives insight into the desired separation angle that should be used. For example, the desired phase separation should be kept small if bearings-only sensors are used with a control policy that allows the standoff range to vary. Conversely, the sensitivity analysis can indicate which sensor type is better for a given control policy. Because autopilots and sensor

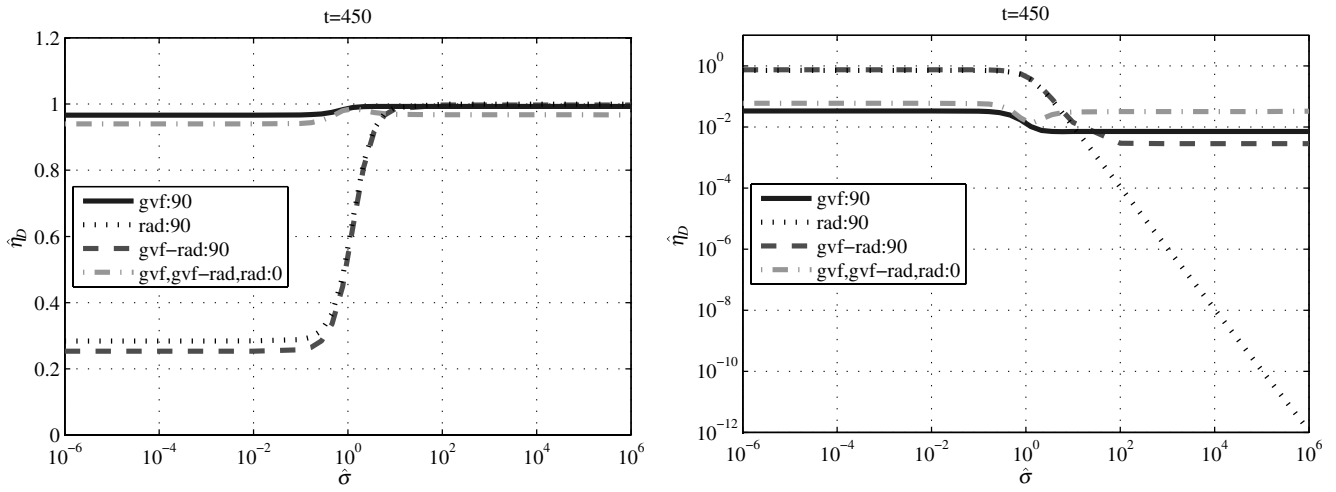

Fig. 11 Final information cost (at time 450 s) vs $\hat{\sigma}$: a) semilog plot of information cost, b) log plot of information error ($1 - \hat{\eta}_{450}^{\mu}$).

packages are often designed by different manufacturers, there is an appropriate choice for each, given a target geolocalization scenario.

When using the FIM to design optimal sensing systems, it is important to recognize several fundamental limitations of the approach. The FIM is calculated based on the true target state and only provides a bound on estimator performance. In general, geolocalization using range and bearing sensors cannot be assumed to achieve the Cramer–Rao lower bound. Thus, the FIM cannot be used to predict estimator performance. Rather, it can be used to compare the expected performance of different coordination or control policies. An alternative design approach is to simulate implementation of a specific geolocalization algorithm and compare its performance for different coordination policies. This approach has the advantage of predicting the actual geolocalization performance, but does not generalize to other estimation algorithms.

The analysis described in this article has several other limitations that must be considered when applying the results to orbit coordination design. First and foremost, the use of the nondimensionalized sensor standard deviation $\hat{\sigma}$ contains several hidden simplifications. The sensor model presented here with Gaussian measurement noise ignores the fact that range measurements must always be positive, i.e., in front of the sensor, and in the sensor field of view. Furthermore, the nondimensional variance masks the actual sensor performance. In cases where the bearing and range components of the measurements are very good (i.e., low uncertainty), adequate performance in terms of actual error bounds could be obtained for many different coordination schemes. Second, the FIM defined here was based on a deterministic target model. When the target model includes random process noise, e.g., as is typical of estimators for moving targets, the posterior Cramer–Rao lower bound must be used [29]. However, the analysis presented here still captures the general trends and can be used as a tool for designing the orbit coordination policies. Third, additional costs such as fuel usage or power expended to turn the UAS, as opposed to accelerate it, were not discussed. Future work could incorporate these terms into more advanced cost functions. Finally, the orbit coordination policies described here should be compared against optimal coordination algorithms for tracking a moving target with background wind under control limitations [10].

VII. Conclusions

This paper studied the sensitivity of cooperative target geolocalization to orbit coordination. Target geolocalization by two cooperating unmanned aircraft with bearing and range sensors improves estimation performance over a range of sensor characteristics. The optimal configuration for a single set of combined measurements was derived over the complete set of possible sensor characteristics. This configuration consists of orbiting the target point at the minimum possible range and with unmanned aircraft phase separation of 90 deg.

Although the optimal configuration is straightforward to calculate, it is difficult to maintain in practice by unmanned aircraft in realistic flight modes. Target velocity and background wind can easily lead to infeasible requirements for a team of unmanned aircraft trying to coordinate flight to maintain the optimal configuration. Thus, different orbit coordination algorithms trade relative phasing and range to target, and the sensitivity of geolocation error to orbit coordination errors is important in designing robust cooperative tracking.

To generalize the discussion of orbit coordination and geolocalization error, a nondimensional optimality criterion was developed based on the determinant of the Fisher information matrix of the geolocalization problem. Analysis revealed that the sensitivity of this criterion is a nonlinear function of the (nondimensional) system states and a nondimensional measurement standard deviation term $\hat{\sigma}$. For small values of $\hat{\sigma}$, corresponding to bearings-only tracking, the cost criterion is more sensitive to range than phasing. For $\hat{\sigma} = 1$, the Fisher information matrix, and thus the optimality criterion, is independent of the angular separation between vehicles. Finally, for large values of $\hat{\sigma}$, geolocalization becomes trilateration which is independent of the range of the unmanned aircraft to the target.

The sensitivity of the geolocalization error to measurement variance was verified through simulation results which show that different coordination control algorithms are suitable for different values of $\hat{\sigma}$. However, overall behavior across all values of $\hat{\sigma}$ was better for control policies that maintain range while allowing the phase separation to vary away from the optimal value. Even in situations when the alternative policies performed better, the overall error compared with the ideal control policy was less than 1%. Thus, if a single orbit coordination algorithm must be designed for a unmanned aircraft that could carry sensors of varied capability, maintaining optimal range at the expense of phasing is preferred.

Acknowledgments

The author would like to thank the anonymous reviewers for their helpful comments.

References

[1] Office of the Secretary of Defense, "Unmanned Aircraft Systems Roadmap: 2005-2030," Aug. 2005, p. A-2.

[2] Ousingsawat, J., and Campbell, M. E., "Establishing Trajectories for Multi-Vehicle Reconnaissance," *Collection of Technical Papers: AIAA Guidance, Navigation, and Control Conference*, Vol. 3, AIAA, Reston, VA, 2004, pp. 2188–2199.

[3] Wheeler, M., Wise, R., and Rysdyk, R., "Autonomous Cooperative Geo-Location and Coordinated Tracking of Moving Targets," *AIAA Infotech@Aerospace 2007 Conference and Exhibit*, AIAA, Reston, VA, 2007, pp. 1479–1488.

[4] Frew, E. W., Lawrence, D. A., and Morris, S., "Cooperative Standoff Tracking of Moving Targets Using Lyapunov Guidance Vector Fields," *Journal of Guidance, Control, and Dynamics*, Vol. 31, No. 2, 2008, pp. 290–306. doi:10.2514/1.30507

[5] Rysdyk, R., Lum, C., and Vagners, J., "Autonomous Orbit Coordination for Two Unmanned Aerial Vehicles," *Collection of Technical Papers: AIAA Guidance, Navigation, and Control Conference*, Vol. 6, AIAA, Reston, VA, 2005, pp. 4876–4884.

[6] Wise, R. A., and Rysdyk, R. T., "UAV Coordination for Autonomous Target Tracking," *Collection of Technical Papers: AIAA Guidance, Navigation, and Control Conference*, Vol. 5, AIAA, Reston, VA, Aug. 2006, pp. 3210–3231.

[7] Martinez, S., and Bullo, F., "Optimal Sensor Placement and Motion Coordination for Target Tracking," *Automatica*, Vol. 42, No. 4, 2006, pp. 661–668. doi:10.1016/j.automatica.2005.12.018

[8] Gu, G., Chandler, R. R., and Schumacher, C. J., "Optimum Cooperative UAV Sensing Based on Cramer–Rao Bound," *Proceedings of the 2005 American Control Conference*, Vol. 6, Inst. of Electrical and Electronics Engineers, New York, Sept. 2005, pp. 4090–4095.

[9] Ousingsawat, J., and Campbell, M. E., "On-Line Estimation and Path Planning for Multiple Vehicles in an Uncertain Environment," *International Journal of Robust and Nonlinear Control*, Vol. 14, No. 8, May 2004, pp. 741–766. doi:10.1002/rnc.933

[10] Hernandez, M. L., "Optimal Sensor Trajectories in Bearings-Only Tracking," *Proceedings of the Seventh International Conference on Information Fusion*, Vol. 2, International Society for Information Fusion, Fairborn, OH, 2004, pp. 893–900.

[11] Grocholsky, B., Makarenko, A., and Durrant-Whyte, H., "Information-Theoretic Coordinated Control of Multiple Sensor Platforms," *International Conference on Robotics and Automation*, Vol. 1, Inst. of Electrical and Electronics Engineers, New York, Sept. 2003, pp. 1521– 1526.

[12] Ogren, P., Fiorelli, E., and Leonard, N. E., "Cooperative Control Of Mobile Sensor Networks: Adaptive Gradient Climbing in a Distributed Environment," *IEEE Transactions on Automatic Control*, Vol. 49, No. 8, Aug. 2004, pp. 1292–1302. doi:10.1109/TAC.2004.832203

[13] Ousingsawat, J., and Campbell, M., "Optimal Cooperative Reconnaissance Using Multiple Vehicles," *Journal of Guidance, Control, and Dynamics*, Vol. 30, No. 1, 2007, pp. 122–132. doi:10.2514/1.19147

[14] Ucinski, D., "Optimal Sensor Location for Parameter Estimation of Distributed Processes," *International Journal of Control*, Vol. 73,

No. 13, 2000, pp. 1235–1248.
doi:10.1080/002071700417876

[15] Chung, T. H., Gupta, V., Burdick, J. W., and Murray, R. M., "On a Decentralized Active Sensing Strategy Using Mobile Sensor Platforms in a Network," *43rd IEEE Conference on Decision and Control*, Vol. 2, Inst. of Electrical and Electronics Engineers, New York, Dec. 2004, pp. 1914–19.

[16] Kalandros, M. and Pao, L. Y., "Covariance Control for Multisensor Systems," *IEEE Transactions on Aerospace and Electronic Systems*, Vol. 38, No. 4, 2002, pp. 1138–1157.
doi:10.1109/TAES.2002.1145739

[17] Passerieux, J. M., and Cappel, D. V., "Optimal Observer Maneuver for Bearings-Only Tracking," *IEEE Transactions on Aerospace and Electronic Systems*, Vol. 34, No. 3, 1998, pp. 777–788.
doi:10.1109/7.705885

[18] Huster, A., Frew, E. W., and Rock, S. M., "Relative Position Estimation for AUVs by Fusing Bearing and Inertial Rate Sensor Measurements," *Oceans 2002 Conference and Exhibition. Conference Proceedings*, Vol. 3, Inst. of Electrical and Electronics Engineers, New York, Oct. 2002, pp. 1863–70.

[19] Grocholsky, B. P., Swaminathan, R., Kumar, V., Taylor, C. J., and Pappas, G. J., "Coordinated Perception by Teams of Aerial and Ground Robots," *Proceedings of the SPIE: The International Society for Optical Engineering*, Vol. 5609, No. 1, 2004, pp. 181–191.
doi:10.1117/12.571769

[20] Frew, E. W., "Receding Time Horizon Control Using Random Search for UAV Navigation with Passive, Non-Cooperative Sensing," *Collection of Technical Papers: AIAA Guidance, Navigation, and Control Conference*, Vol. 1, AIAA, Reston, VA, Aug. 2005, pp. 553–565.

[21] Frew, E. W., "Receding Horizon Control Under Uncertainty Using Optimal Input Design and the Unscented Transform," *45th IEEE Conference on Decision and Control*, Inst. of Electrical and Electronics Engineers, New York, Dec. 2006, pp. 4830–4835.

[22] Frew, E., Dixon, C., Argrow, B., and Brown, T., "Radio Source Localization by a Cooperating UAV Team," *AIAA Infotech@Aerospace*, Vol. 1, AIAA, Reston, VA, Sept. 2005, pp. 10–20.

[23] Sepulchre, R., Paley, D. A., and Leonard, N. E., "Stabilization of Planar Collective Motion: All-to-All Communication," *IEEE Transactions on Automatic Control*, Vol. 52, No. 5, 2007, pp. 811–824.
doi:10.1109/TAC.2007.898077

[24] Campbell, M. E., and Wheeler, W., "Vision Based Geolocation Tracking System for UAVs," *AIAA Guidance, Navigation, and Control Conference*, Vol. 3, AIAA, Reston, VA, 2006, pp. 1942–1959.

[25] Dobrokhodov, V. N., Kaminer, I. I., and Jones, K. D., "Vision-Based Tracking and Motion Estimation for Moving Targets Using Small UAVs," *AIAA Guidance, Navigation, and Control Conference*, Vol. 7, AIAA, Reston, VA, 2006, pp. 4389–4400.

[26] Barber, D. B., Redding, J. D., and McLain, T. W., "Vision-Based Target Geo-Location Using a Fixed-Wing Miniature Air Vehicle," *Journal of Intelligent and Robotic Systems: Theory and Applications*, Vol. 47, No. 4, 2006, pp. 361–382.
doi:10.1007/s10846-006-9088-7

[27] Taylor, J. H., "Cramer–Rao Estimation Error Lower Bound Computation for Deterministic Nonlinear Systems," *IEEE Transactions on Automatic Control*, Vol. AC-24, No. 2, April 1979, pp. 343–4.

[28] Atkinson, A. C., and Donev, A. N., *Optimum Experiment Designs*, Clarendon, London, 1992.

[29] Tichavsky, P., Muravchik, C., and Nehorai, A., "Posterior Cramer–Rao Bounds for Discrete-Time Nonlinear Filtering," *IEEE Transactions on Signal Processing*, Vol. 46, No. 5, 1998, pp. 1386–1396.
doi:10.1109/78.668800